Title	Effect of surface and defect chemistry on the photo-catalytic properties of intentionally defect-rich ZnO nanorod arrays
Author(s)	Kegel, Jan; Zubialevich, Vitaly Z.; Schmidt, Michael; Povey, Ian M.; Pemble, Martyn E.
Publication date	2018-05-08
Original citation	Kegel, J., Zubialevich, V. Z., Schmidt, M., Povey, I. M. and Pemble, M. E. (2018) 'Effect of surface and defect chemistry on the photo-catalytic properties of intentionally defect-rich ZnO nanorod arrays', ACS Applied Materials and Interfaces. doi:10.1021/acsami.8b05130
Type of publication	Article (peer-reviewed)
Link to publisher's version	http://dx.doi.org/10.1021/acsami.8b05130 Access to the full text of the published version may require a subscription.
Rights	© 2018, American Chemical Society. This document is the Accepted Manuscript version of a Published Work that appeared in final form in ACS Applied Materials and Interfaces after technical editing by the publisher. To access the final edited and published work see https://pubs.acs.org/doi/abs/10.1021/acsami.8b05130
Embargo information	Access to this article is restricted until 12 months after publication by request of the publisher.
Embargo lift date	2019-05-08
Item downloaded from	http://hdl.handle.net/10468/6123

University College Cork, Ireland
Coláiste na hOllscoile Corcaigh

Energy, Environmental, and Catalysis Applications

Effect of Surface and Defect Chemistry on the Photo-catalytic Properties of Intentionally Defect-rich ZnO Nanorod Arrays

Jan Kegel, Vitaly Z. Zubialevich, Michael Schmidt, Ian M. Povey, and Martyn E. Pemble

Just Accepted

Effect of Surface and Defect Chemistry on the Photo-catalytic Properties of Intentionally Defect-rich ZnO Nanorod Arrays

Jan Kegel[a,*], Vitaly Z. Zubialevich[a], Michael Schmidt[a], Ian M. Povey[a], Martyn E. Pemble[a,b]

[a] Tyndall National Institute, University College Cork, Lee Maltings, Cork, Ireland.
[b] Department of Chemistry, University College Cork, Cork, Ireland.

ABSTRACT: Due to the abundance of intrinsic defects in zinc oxide (ZnO) the material properties are often governed by same. Knowledge of the defect chemistry has proven to be highly important, especially in terms of the photo-catalytic degradation of pollutants. Given the fact that defect-free materials or structures exhibiting only one type of defect are extremely difficult to produce, it is necessary to evaluate what influence various defects may have when present together in the material. In this study, intentionally defect-rich ZnO nanorod (NR) arrays are grown using a simple low-temperature solution-based growth technique. Upon changing the defect chemistry using rapid thermal annealing (RTA) the material properties are carefully assessed and correlated to the resulting photo-catalytic properties. Special focus is put on the investigation of these properties for samples showing strong orange photoluminescence (PL). It is shown that intense orange emitting NR arrays exhibit improved dye-degradation rates under UV-light irradiation. Furthermore strong dye-adsorption has been observed for some samples. This behavior is found to stem from a graphitic surface structure (e.g. shell) formed during RTA in vacuum. Since orange-luminescent samples also exhibit an enhancement of the dye-adsorption a possible interplay and synergy of these two defects is elucidated. Additionally, evidence is presented suggesting that in annealed ZnO NRs structural defects may be responsible for the often observed PL emission at 3.31 eV. However, a clear correlation with the photo-catalytic properties could not be established for these defects. Building on the specific findings presented here, this study also presents some more general guidelines which it is suggested, should be employed when assessing the photo-catalytic properties of defect-rich ZnO.

Introduction

Governed by its low-cost, environmentally friendly and earth-abundant nature ZnO represents a promising material to be used in various applications such as gas sensing,[1, 2] light emitting diodes,[3-6] photovoltaics as well as photo-(electro)chemical (PEC) applications.[7-15] In these applications the material performance is dramatically influenced by intrinsic defects. As-deposited ZnO commonly presents intrinsic defects, whereby the density and nature of same crucially depends on the deposition technique and deposition environment used.[16-18] Interestingly, several literature reports point out that the existence of intrinsic defects in ZnO does not necessarily lead to poorly performing devices and can in fact enhance the device performance, especially for photo-(electro)chemical applications.[1, 11, 14, 19-22] In the field of photo-catalysis published literature reports suggest that intrinsic defects such as oxygen vacancies V_O and zinc interstitials Zn_i can increase the photo-catalytic activity of prepared ZnO nanomaterials towards model pollutant species, usually dyes of various types.[14, 19, 23-25] These studies have identified the defects either as charge-carrier traps which delay the re-

combination processes of photo-excited charge carriers and/or as surface-sites where the pollutant/dye is degraded via the charge transfer from the pollutant/dye to the defect state. Furthermore, it has recently been shown that strong orange-luminescent ZnO NR arrays – prepared in a similar manner to the samples in this study – can significantly enhance the PEC performance for solar water splitting under simulated solar irradiation.[26] Also in this case an increased charge transfer rate for photo-generated charge carriers (holes) could be observed with the experimental data suggesting that the observed behavior stems from a lower/slower rate of recombination.

Apart from intrinsic defects in the material the activity of ZnO in respect to these PEC reactions can also be influenced by other factors. As summarized by Kumar and Rao, the photo-catalytic properties of ZnO can be significantly affected by e.g. the morphology, crystal facets and their polarity, doping and impurities, surface modification as well as the deposition of multi-material structures.[21] Thus it becomes obvious that the overall photo-catalytic activity of a given ZnO structure is influenced by multiple aspects. Therefore a direct comparison of for example different ZnO morphologies with varying defect composi-

tion is not straight forward, since the exact contribution of each individual aspect (i.e. morphology and intrinsic defects) is difficult to determine.

For this reason, in this present study we aim to minimize the number of possible variables by evaluating a range of intentionally defect-rich ZnO NR arrays, all grown using the same growth-parameters. In order to investigate the interplay of intrinsic defects and their possible influence on the photo-catalytic properties we apply post-deposition rapid thermal annealing (RTA) to vary the defect composition and defect density in the films. Initially the study focuses on the observation of strong orange-emission from samples annealed around 450 °C. It is important to note that careful material characterization (XRD, PL/excitation-PL, UV-Vis, XPS) of similarly deposited ZnO NR arrays has revealed that this defect centre is temperature dependent but annealing atmosphere independent, with the V_O-Zn_i defect-complex being the likely source of the observed orange emission.[26] Building on these earlier results, it is presented that strong dye adsorption depending on the nature of the dye (here methylene blue MB and methyl orange MO are used) can be recognized for some samples annealed at this temperature (450 °C). By means of Raman spectroscopy, transmission electron microscopy (TEM), low temperature PL (LT-PL) and photo-catalytic dye-degradation measurements the extent to which the orange-luminescent defects are responsible for the observed behavior has been evaluated. Additionally the materials characterization reveals the presence of a graphitic shell as well as the appearance of structural defects (related to LT-PL emission at 3.31 eV) following certain RTA treatments.

In this way the influence of the interplay of all these defects (orange-luminescent defects, structural defects and graphitic shell) on the observed photo-catalytic properties of ZnO NR arrays has been elucidated. Based on the experimental results presented in this study, it is suggested that careful defect-engineering can be used to tailor ZnO towards, and enhance the performance of, specific photo-(electro)chemical applications and that a holistic approach involving as many material properties as possible should be employed in order to assess the photo-catalytic performance of defect-rich materials.

Experimental Methods

ZnO seed-layer coated microscope glass slides (25 x 75 mm) were used as the growth substrates. Prior to the seed-layer preparation by atomic layer deposition (ALD) the microscope glass slides were sonicated for 1 h in a mixture of Millipore water (H_2O; 18.2 MΩ), ammonium hydroxide (NH_4OH) and hydrogen peroxide (H_2O_2) in a ratio of H_2O:NH_4OH:H_2O_2 = 5:1:1.

Seed-layer preparation by ALD

Diethylzinc (Sigma Aldrich) and H_2O were used as the precursors for the ALD of seed-layers using a Cambridge NanoTech Fiji F200LLC System. The growth was carried out over 400 cycles (ca. 70 nm film thickness) at 190 °C substrate temperature followed by natural cooling in air.

Subsequently the seed-layer coated substrates were annealed in air for 1 h at 300 °C. 70 nm was deliberately selected as the typical layer thickness since layers of this thickness would most likely prevent possible impurity migration from the substrate into ZnO NRs.

Solution growth of ZnO NR arrays

Intentionally defect-rich ZnO NRs were grown using a solution-based method as presented in Ref [26]. In short: 100 ml of solution were prepared by dissolving and continuous stirring (1 h) of 0.025 M zinc nitrate hexahydrate ($Zn(NO_3)_2$·$6H_2O$, (ZNH), reagent grade) and 0.15 M hexamethylenetetramine ($C_6H_{12}N_4$, (HMTA), reagent grade) and 4 drops of 5 %wt hydrochloric acid (HCl, reagent grade) in H_2O. As presented by Ranjith et al., a high HMTA to ZNH concentration ratio allows thereby for the deposition of ZnO rich in intrinsic defects – especially Zn_i.[13] Afterwards the solution was transferred into a sealable plastic bottle and seed-layer coated substrates were immersed into the solution. The substrates where placed almost vertically and the growth side was pointing slightly downwards. Subsequently the sealed bottle was heated to 95 °C in a standard laboratory oven. After the growth period (6 h) the naturally cooled solution was discarded and the obtained samples were thoroughly rinsed with H_2O and blow dried with nitrogen. In order to avoid possible impairment of later photo-catalytic measurements any growth on the backside of the samples was carefully etched back using HCl.

Rapid Thermal Annealing (RTA) of ZnO nanorod-arrays

The ZnO nanorod-arrays were annealed at various temperatures (350 °C, 450 °C, 550 °C) in Oxygen (O_2, 1 bar) and/or in vacuum (VAC)) using a Jipelec 150 RTA system. In the case of oxygen as the annealing atmosphere, the RTA chamber was filled with the gas prior to the temperature ramp up. The samples were then annealed for 10 min at the set temperature (ramp rate = 10 °C/s).

Characterization

Samples were subject to LT-PL analysis at 11.5 K using a cw He-Cd laser (λ_{ex} = 325 nm, 1.6 mW) as the excitation source. A Jeol JEM-2100 was used to record TEM images of ZnO NRs. Raman analysis was performed using a Renishaw micro-Raman spectrometer equipped with a 514 nm laser. The beam was focused trough a Leica 100 x (NA = 0.9) objective. The laser power density on the sample was less than 5 mW/μm^2 (spot size ca. 1 μm).

The photo-catalytic properties were tested by placing a ZnO NR array into a UV-cuvette filled with 3 ml of ca. 17 μM methylene blue solution (MB) or ca. 55 μM methyl orange solution (MO) in H_2O. The absorbance spectrum of the constantly stirred dye solution was then monitored at 664 nm (MB) or 464 nm (MO) every 20 seconds using an Ocean optics HL-2000-LL lamp and QE65000 spectrophotometer. During a typical analysis the dye solution was left in the measurement setup for at least 30 min in the dark prior to the insertion of the sample. The last absorbance measurement before the sample was put into the solution was taken to determine the initial dye concentration C_0 (Lambert–Beer law). After the sample was

put into the cuvette the dark dye-adsorption was measured for 1.5 h after which the illumination was turned on. This "light on" stage lasted for 1.5 h followed by another off/on cycle (1 h each). Finally an additional "light off" stage was introduced for 20 min. A 365 nm high power UV-LED has been used as light source. The intensity has been adjusted to either 1 mW/cm² (low-intensity; l.i.) or 3 mW/cm² (high-intensity; h.i.). Since multiple photo-catalytic measurements have been performed on each sample, the results presented have been labelled in accordance to the number of measurements the sample had been subjected to (e.g. (1) for the first, (2) for the second photo-catalytic measurement etc.). Between the photo-catalytic measurements the samples were washed in ethanol and Millipore water (30 min each).

It is important to note that the real surface area of the samples could not be determined. Hence, sample comparisons on the basis of the absolute changes of the dye concentration are not meaningful. The reader should therefore evaluate each dye-degradation diagram presented as an individual measurement sequence. Since all the measurements in one dye-degradation plot are taken on the same sample (if not mentioned otherwise), knowledge of the exact surface area is not necessary. This approach allows us to draw conclusions regarding the general trends among the samples (e.g. dark dye-adsorption, changes in the photo-catalytic activity upon annealing etc.). Furthermore absolute comparisons of the dye-degradation performance between measurements on the same sample are possible. Because of the latter, dye-degradation rates for each measurement have been calculated from the first "light on" stage. In order to avoid confusion (i.e. unwanted sample comparison) these rates are listed in Table S1 and Table S2.

Furthermore it is important to make the reader aware of the shortcomings that dye discoloration-tests may represent when evaluating the photo-catalytic performance of materials. A major drawback – especially when investigating visible light active materials – is that dyes may also absorb visible light. This can induce e.g. self-decomposition or dye-sensitization of the photo-catalyst leading to a discoloration of the solution that may then be misinterpreted to stem from the photo-catalyst.[27-29] Similarly, in the case of MB, discoloration may also occur due to the reduction of MB to the leuco methylene blue form (LMB). Since LMB is only an intermediate and can be readily form MB again when oxygen is present in the solution (pH dependent) the dye is not fully degraded and discoloration rates may be again misleading.[27] Also the charge of the dye is crucial, as attractive forces between the photo-catalyst and dye can lead to higher degradation rates. The pH of the dye solution may even intensify this effect.[27, 29] In the present study the aforementioned effects were minimized by choosing 365 nm as illumination wavelength (no/little absorption of the MB and MO but full absorption of ZnO, see Figure S1), performing the tests in nearly neutral solution (less "artificial" dye adsorption) and light on/off cycling. The latter allows examining a possible re-colorization which can be an indication of a not fully degraded dye (e.g. LMB formation for MB decomposition). Finally it is important to point out that while it is certainly true that the dye testing can be influenced by many factors, for the purpose of the present study, comparative measurements were carried out only. These were done on a series of materials that are all essentially the same in terms of structure, bulk composition and morphology. Our materials differ only in the number and nature of the defects present.

Results and discussion

Prior to the RTA treatment various samples were evaluated for the reproducibility of the described deposition method. Furthermore the material characterization depicted in Fig S2 was carried out to ensure that no major differences between the samples exist. As visible from the PL, XRD and SEM measurements in Figure S2, the synthesis procedure leads to comparable NR array growth - structurally as well as optically in terms of their overall defect emission shape.

In an earlier study it was demonstrated that RTA at temperatures of *ca.* 450 °C leads to strong, defect-related orange emission, from samples prepared using the growth method outlined in this paper. These defects occurred regardless of the annealing atmosphere used (argon, oxygen, forming gas, nitrogen, vacuum) and represented the dominating recombination channel in these structures.[26]

Fueled by these earlier results photo-catalytic measurements on a set of samples, annealed at 450 °C in contrasting RTA conditions – vacuum and oxygen, have been carried out. The defect-related orange emission was readily observed for both of the annealed samples (Figure 1 a)). While the as-grown sample shows deep-level defect (DLD) emission one order of magnitude smaller than the near-band-edge (NBE) emission, the DLD/NBE intensity ratio drastically increased for both samples subjected to RTA at 450 °C. The DLD-related peak for these samples was centered around 1.9 eV (orange) with two smaller shoulders being noticeable in the range 2.6 eV – 2.1 eV. The DLD emission spectrum was fitted with 3 Gaussian peaks indicating that the orange emission at 1.9 eV was responsible for more than 90 % of the total intensity (see Figure S3).

Additionally the RTA treated samples exhibited clear features in the NBE emission with peaks at ca. 3.375 eV, 3.363 eV, 3.313 eV, 3.240 eV and 3.170 eV. For the as-grown sample only a broad peak at ca. 3.363 eV and a sub-bandgap emission centered around 3.225 eV could be noticed.

Figure 1 a) already includes the assignment of the observed NBE peaks stemming from a detailed discussion in a later section of this paper. For the moment it is only important to note the following: RTA at 450 °C leads to the emergence of strong defect-related orange emission with intensity on the same order of magnitude as the NBE – regardless of the annealing atmosphere used. Furthermore contrasting RTA conditions do not influence the
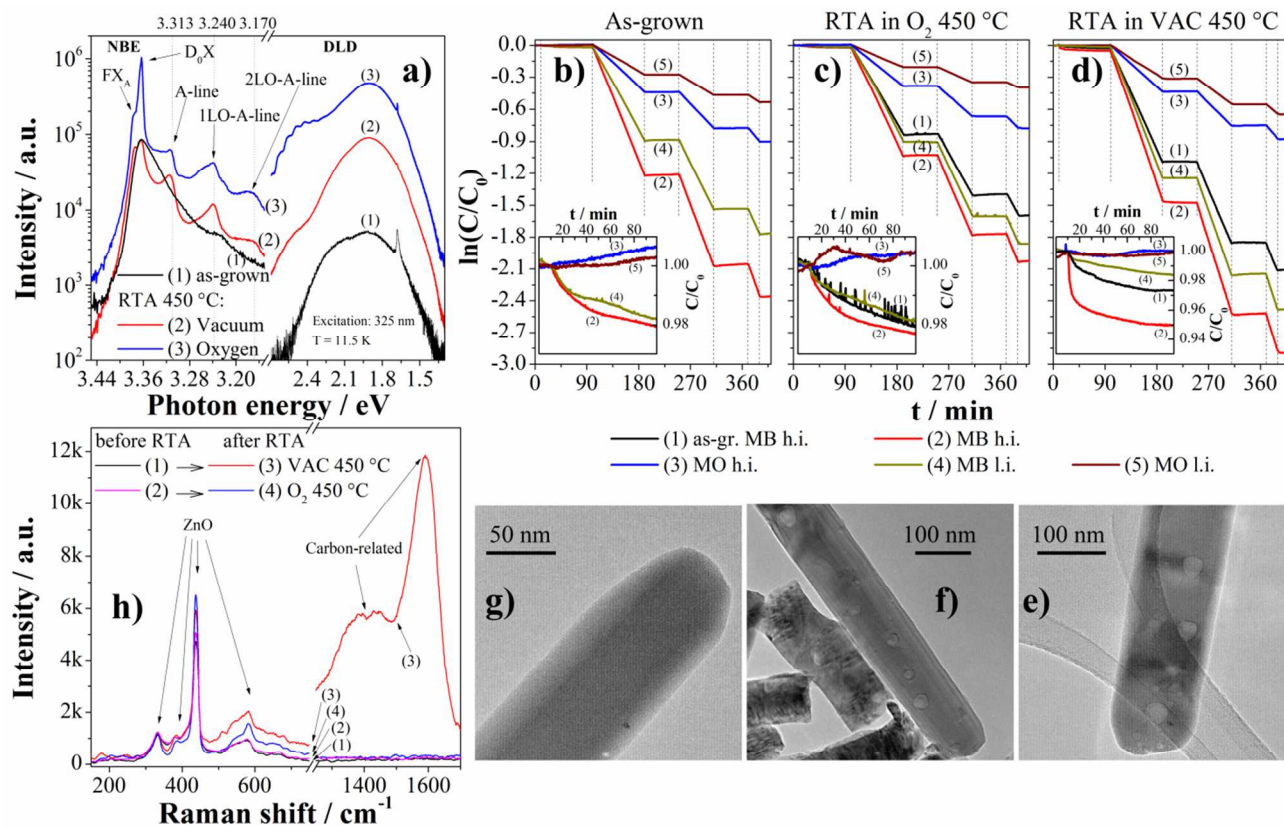
Figure 1. Materials characterization for as-grown and RTA treated (450 °C; in vacuum or oxygen) ZnO NR arrays. a) LT-PL spectra of as-grown + RTA treated ZnO NR arrays. b) - d) dark dye-adsorption and photo-catalytic dye-degradation curves in methylene blue (MB) and methyl orange (MO) for as-grown + RTA treated samples. Insets show the change of the dye concentration in the first dark stage magnified. Dye-degradation was carried out under illumination from a UV-LED (365 nm) with high intensity (3 mW/cm²; h.i.) or low intensity (1 mW/cm²; l.i.). Corresponding TEM micrographs of annealed ZnO NR arrays: e) VAC 450 °C, f) O₂ 450 °C and g) as-grown ZnO nanorod. h) Raman spectra of ZnO nanorod arrays before and after RTA in O₂ or VAC at 450 °C revealing the presence of a graphitic structure in the case of vacuum as annealing atmosphere (e.g. shell/layer or clusters).

appearance of characteristic peaks in the NBE emission. These peaks and their positions are essentially the same for the samples annealed in oxygen or vacuum.

With the knowledge of the changes in defect chemistry that results from the RTA – especially in regards to the strong orange DLD emission – the samples have been analyzed for their photo-catalytic properties. First an as-grown sample has been analyzed. Its photo-catalytic properties are shown in Figure 1 b). When the sample is put into the solution (after initial stage without sample – dye solution only) the concentration is observed to decrease when MB is the dye used. On the other hand, virtually no change in the dye-concentration can be noticed when methyl orange (MO) is used as the dye. However, MB is known to be easily adsorbed to various surfaces. Thus it is possible that the dye is also attracted by the substrate. Therefore the adsorption of MB cannot conclusively being attributed to the ZnO nanorod-arrays alone. It is noteworthy that the dark-adsorption is very similar for the two measurements performed on the sample, indicating the acceptable level of reproducibility of the measurement.

After turning on the UV-LED both dyes are degraded by the ZnO nanorod-arrays, as evidenced by a decreasing C/C₀ ratio. The difference in the magnitude of degradation between the two dye solutions used is related to the higher concentration of MO compared to MB. When comparing the photo-catalytic dye-degradation of the sample under high ((curves (2) and (3) in Figure 1 b)) and low intensity (curves (4) and (5) in Figure 1 b)), it can be seen that for MB (cationic) as well as for MO (anionic) a higher illumination intensity leads to faster dye-degradation.

Under the assumption that a higher illumination intensity leads to a higher photo-generated charge carrier density, the measurements suggest that the increased photo-catalytic activity is due to an increased charge carrier transfer at the dye solution/ZnO interface. The exact mechanism of dye-degradation is not the topic of this study but studies on both systems ZnO/MO and ZnO/MB conclude that photo-generated holes in the valence band and photo-generated electrons in the conduction band (and trapped at defect sides) contribute to the dye-degradation.[21, 30-33] However, for MB an assessment of the formation of dye-intermediates is to a certain extent pos-

sible by evaluating the dark stage after the first illumination stage. If the bleaching of the dye solution is caused due to the formation of the leuco methylene blue form (LMB) over the reduction of MB by electrons from the conduction band from ZnO, a recovery of the C/C_o ratio should be observed during this stage. In a dark, well aerated system (in this study constant stirring) LMB would thereby rapidly react with oxygen to form MB thus leading to the recovery.[27, 34] The fact that a strong recovery of the MB concentration is not observed indicates that this degradation mechanism is not dominant for the samples. However, it is important to note that the re-oxidation to MB may be considerably slower in the case of LMB bonded to OH^- groups (e.g. bound to the nanorod surface).[35] On a longer time scale, the binding of LMB to the nanorod surface could in turn lead to photo-catalyst poisoning, as also observed for other intermediates of the ZnO-MB system.[36]

The dye-degradation curves for the samples subjected to RTA in O_2 and vacuum at 450 °C are shown in Figure 1 c) and d), respectively. In order to evaluate the influence of RTA on the photo-catalytic performance the samples were also studied prior to the heat treatment. These curves (black traces (1) in Figure 1 c) and d)) show a similar behavior among all stages of the experiment when compared to the as-grown sample in Figure 1 b).

After RTA both samples show an improved photocatalytic dye-degradation of MB and MO. For the orange-luminescent samples a higher number of charge carriers have thus to be present at the surface in order to facilitate the catalytic reactions. Since the defect-related recombination in these samples is dominant this must in turn mean that recombination itself involves slow-trapping of a photo-generated electron to increase the lifetime of the photo-generated hole or that the defect states are active towards dye degradation themselves.

When comparing these two samples, it is however noticed that the sample annealed in vacuum shows a strong dark adsorption of MB. The first dark stage is magnified for these samples in Figure 1 c) and d). For the first measurement after RTA (trace (2) – red; MB) a strong decrease of the dye concentration is visible for the sample annealed in vacuum. Interestingly no dark absorption could be observed for the measurements in MO solution. Since the dark adsorption is so different for dyes with different polarity it seems appropriate to reason that the surface of the nanorod-arrays annealed in vacuum at 450 °C must exhibit some sort of charge – in this case negative.

From the results presented so far it is concluded that the observed dye-adsorption is not directly related to any of the observed PL features. It is not related either to the strong orange emission nor to the defect centres responsible for the features in the NBE ("A-lines") because if it were, then the sample annealed in oxygen would show a similar dark dye-adsorption.

Furthermore it is noteworthy that after RTA both annealed samples degrade MB faster under low intensity illumination (1 mW/cm², curves (4) in Figure 1 c) and d)) than compared to measurements under high intensity illumination but before RTA (3 mW/cm², curves (1) in Figure 1 c) and d)). Thus it may be possible that due to the relatively low MB concentration of *ca.* 17 μM the dye-degradation at higher illumination intensities might be somewhat mass transport limited.

In order to get a better understanding of what governs the observed photo-catalytic properties TEM (Figure 1 e) – g)) and Raman analysis (Figure 1 h)) have been carried out on these samples. Focusing on the TEM image of an as-grown NR first (Figure 1 g)) no obvious structural defects can be observed. This situation changes upon RTA. Here structural defects can be seen for both vacuum and O_2 as the annealing atmospheres (Figure 1 e) and (Figure 1 f), respectively). The defects are visible throughout the entire length of the rods and also the density of the defects seems to be independent of the annealing atmosphere used. A closer evaluation and correlation of the structural defects to the PL properties is carried out in a later section. However, for the moment it is important to note the appearance of the structural defects in both annealed sample does in turn indicate that these defects can also not be responsible for the strong dye-adsorption in the dark of the vacuum annealed sample.

The Raman measurements shown in Figure 1 h) were initially taken to a) confirm the deposition of hexagonal NRs and b) to look for possible manifestations of defects in the spectra. In short, the modes seen in the range 150 – 750 cm⁻¹ can indeed be all attributed to wurzite ZnO while no meaningful information may be gathered regarding the nature of any intrinsic point defects.[37-40] However, it is noteworthy that the intensity of the dominant $E_2(H)$ mode (ca. 439 cm⁻¹) is increased after both RTA treatments. Generally, an increase in the peak intensity is associated with an improvement of the crystal quality.[20] When comparing the $A_1(LO)$ mode (broad feature around 580 cm⁻¹) for both annealed samples, it can be additionally noticed that the sample annealed in vacuum exhibits and increased intensity. Since this mode is commonly associated with oxygen deficiency it may be reasonable to expect a slight increase in the concentration of oxygen vacancies upon RTA in vacuum.[20, 41, 42] Also the intensity of the collected spectra does not differ strongly for the respective samples. However, a surprising observation was made while scanning to longer Raman shifts (right part in Figure 1 h)). While all other samples showed no response for Raman shifts > 750 cm⁻¹ the sample which has been annealed in vacuum at 450 °C exhibits a strong Raman signal in the range 1250 – 1700 cm⁻¹.

These signals cannot be assigned to ZnO but are in fact carbon-related modes that have been observed by other authors.[43-46] The peak centred around 1590 cm⁻¹ originates from the G-band (graphitic or graphene-like) and the shoulder between ca. 1300 – 1500 cm⁻¹ is the manifestation

5

of the D-band (disordered/defective carbon).[43, 46] From previous XPS measurements on samples prepared in a similar fashion to the samples in this study, it is known that such films are rich in carbon.[26] However, the concentration of carbon in the films (carbon residues as well as unintentional doping) has been found to be comparable for all samples grown and independent of the annealing atmosphere used. An example XPS spectrum (after prolonged argon bombardment for surface contamination removal) of a NR array annealed in vacuum at 450 °C is shown in Figure S4. The high carbon concentration in the films is believed to originate from the high HMTA concentration in the growth solution. As reported previously, the high amount of HMTA is needed for the synthesis of intentionally defect rich NR arrays.[26]

Given the higher intensity of the G-band in the Raman measurements, RTA in vacuum at 450 °C must therefore lead to the formation of Raman active graphitic but defect-rich structures (e.g. layer or clusters) in or around the ZnO nanorods. From this first set of samples multiple questions regarding the influence of defects on the photo-catalytic properties of the ZnO nanorod-arrays persist:

- Is the improved photo-catalytic performance unique to orange-luminescent ZnO NRs or is the improvement only due the annealing treatment itself?
- May oxygen vacancies be responsible for the improved dye-degradation as they have been shown to aid photo-catalytic processes?[23, 47]
- Are the structural defects unique to orange-luminescent ZnO NRs and do they affect the photo-catalytic properties?
- What causes the strong dark dye-adsorption for RTA in vacuum and is the observed graphitic structure somehow linked to it?

In order to evaluate these questions another set of samples was annealed in vacuum but at multiple temperatures. These samples were then measured with respect to their physical and photo-catalytic properties. The samples were then re-characterized following a second RTA treatment in oxygen at 380 °C. Furthermore a lower illumination intensity (1 mW/cm²) was chosen for the photo-catalytic experiments since the measurements with varying intensities and MB as dye in Figure 1 indicated a possible mass transport limitation for the reaction performed using higher illumination intensities.

Before turning to the photo-catalytic properties, we shall however examine first what the nature of the observed structural defects and orange emission may be. The LT-PL spectra of the second set of samples are shown in Figure 2 a)-d). These spectra are again divided between NBE- and DLD-related bands.

Starting with the DLD emission of the samples annealed in vacuum only (Figure 2 b)-d)), it can be seen that the emission changes significantly depending on the RTA temperature. While the intensity of the DLD band is comparably low for the samples annealed at 350 °C and 550 °C, very strong orange emission can be seen at 450 °C. Upon RTA at 550 °C additional defects are introduced centred around 2.5 eV. Given that vacuum was used as the annealing atmosphere it appears likely that these defects stem from the oxygen sub-lattice (e.g. oxygen vacancies). Additionally it is important to note, that annealing at temperatures > 400 °C results in the desorption of hydrogen.[48] Hydrogen, however, can passivate deep-level defects and a possible desorption may thus lead to the emergence/increase of PL emissions in the visible region (especially green) and a decrease of the NBE.[49-51] For further discussion on the DLD emission of comparable samples the reader is referred to Ref. [26]

In light of the appearance of strong orange emission upon RTA at 450 °C it is however important to point out that this defect-emission is observed independent of the RTA atmosphere used (e.g. forming gas, argon, oxygen, vacuum). PL spectra of samples annealed in argon and forming gas are thus presented in Figure S3 and Figure S5, respectively. Furthermore the sample presented in Figure S5 was investigated for the possible diffusion of oxygen vacancies towards the nanorod surface upon annealing treatments, as recently suggested by Bora et al..[52] For the presented samples this effect could however not be as clearly observed as in the mentioned literature report. Importantly the analysis revealed that long-term annealing prior and after the RTA treatment does neither affect the appearance of the orange emission nor does any of the annealing treatments have significant influence on the structural properties of the NRs (e.g. the surface are remains comparable after RTA).

Cross-annealing in oxygen leads to a slight increase of the orange emission for the sample which had been previously subject to RTA in vacuum at 350 C. No change of the emission shape is recognized for the sample which already showed strong orange emission. This is an important finding as it illustrates that the orange emission cannot be eliminated due to annealing in contrasting conditions (oxidizing and reducing). It further underlines a possible kinetic formation of this defect-centre as function of the RTA temperature. For the sample which was first annealed in vacuum at 550 °C the intensity of the emission at ca. 2.5 eV is reduced upon cross-annealing. This may point towards a possible filling of oxygen vacancies at the NR surface due to annealing in oxygen.

When focusing on the NBE, peaks at ca. 3.375 eV, 3.363 eV, 3.313 eV, 3.240 eV and 3.170 eV are again visible for all annealed samples. The peaks seem to become more pronounced with increasing RTA temperature. This is especially true when comparing the different spectra of samples annealed in vacuum at 350 °C and 450 °C (Figure 2 b) and c)), respectively. However, a further temperature increase (550 °C in Figure 2 d)) does not lead to an additional increase in the NBE features.
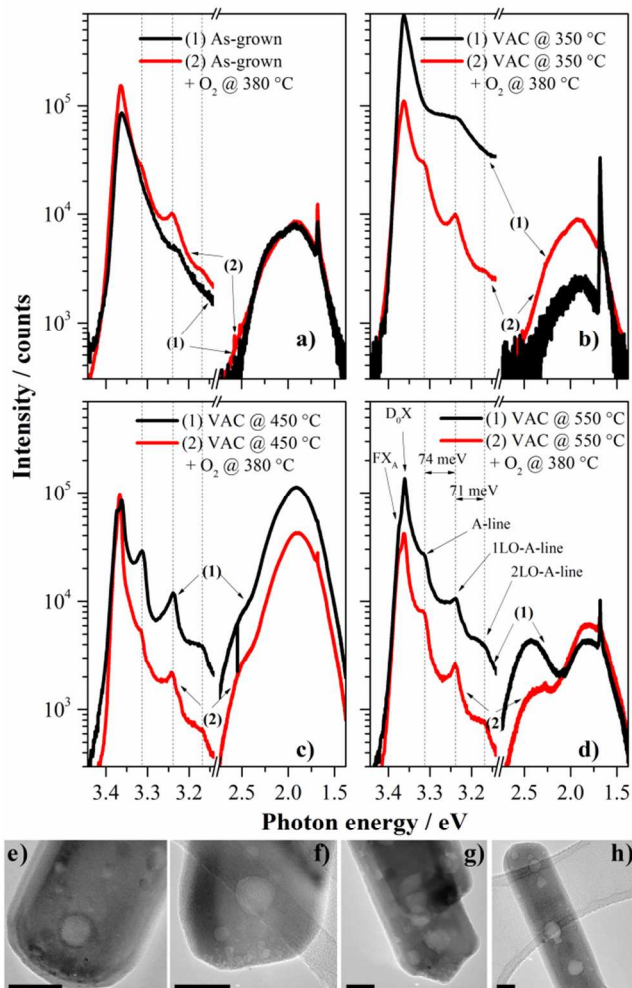
6

Figure 2. a)-d) LT-PL spectra of ZnO NR arrays before and after RTA in O_2 at 380 °C. Samples shown in b)-d) were subject to RTA in vacuum at 350 °C, 450 °C or 550 °C, respectively. Please note that the spectra contain an artefact at ca. 1.68 eV originating from the second harmonic of the NBE peak at ca. 3.363 eV. e)-g) TEM images of the samples annealed in vacuum at 350 °C, 450 °C or 550 °C, respectively. h) TEM image of a NR which had been RTA treated in VAC @ 450 °C and subsequently in O_2 at 380 °C. The scale bar in the images represents 50 nm.

The peaks centred around 3.375 eV and 3.363 eV can be assigned to free excitonic recombination (A-exciton, FX_A) and transitions of excitons bound to neutral donors D_oX, respectively.[53, 54] The presence of an undefined NBE peak, as is the case for the as-grown sample, implies that the NRs are highly defect-rich after the deposition. Especially the FX_A, which gets more pronounced with higher annealing temperatures, indicates an overall improvement of the crystallinity upon RTA. However, the RTA also leads to the emergence of the peaks at ca. 3.313 eV, 3.240 eV and 3.170 eV, which are not located in the two electron satellite region.[54] These peaks show a separation of 74 meV and 71 meV (see Figure 2 d)) which is close to the optical phonon energy in ZnO (72 meV). It is therefore reasona-

ble to assign the peaks at 3.240 eV and 3.170 eV as 1st and 2nd longitudinal optical phonon (LO) replica of the peak at 3.313 eV, which is termed as the "A-line". The A-line luminescence features are often observed in ZnO but their origin is still controversial.[55-59] Based on the optical phonon energy it becomes obvious that the A-line cannot be the phonon replica of the FX_A since the energy difference is too little (62 meV). The appearance of the A-lines is annealing atmosphere independent (see also Figure 1 a)) and also cross-annealing in oxygen at 380 °C does not show any influence on these features. Furthermore it is important to note that the A-line emission is also not related to the observed DLD emission – especially with respect to the orange emission which was found to be annealing atmosphere independent but temperature dependent.

Interestingly the A-line emission coincides with the appearance of structural defects throughout the nanorods. As can be seen from the TEM images of the samples annealed in vacuum at 350 °C, 450 °C and 550 °C (Figure 2 e)-g), respectively) these structural defects are present on/in all of the annealed samples. Furthermore the TEM analysis revealed the presence of these defects throughout the entire rod (bulk and surface) and along the full length, indicating that their appearance is growth-stage independent. Also the structural defects are not influenced by subsequent RTA in oxygen (see example TEM image of a nanorod form a sample annealed in VAC 450 °C + O_2 380 °C in Figure 2 h).

Some structural defects are shown in more detail in Figure 3. The crystal lattice can clearly be seen for both an as-grown as well as an annealed sample (Figure 3 a) and b), respectively). For the as-grown NR-tip no obvious inclusions or impurities are recognized. This is in contrast to the NR depicted in Figure 3 b), which exhibits structural defects. A lighter contrast, as seen for all of these defects, results from an increased transmission trough the rods. This in turn may identify the defects as areas with less material. A hypothesis which is further supported by the fact that the crystal structure inside and around the rod is unchanged (Figure 3 b)). The "real" position of the electronic defect is therefore believed to reside at the edges of the lighter area – visible by a darker outline where the crystal lattice appears to be damaged.

A dark outline and the related lattice damage are also clearly visible for the defect shown in Figure 3 c) – especially in the upper part of the defect. However, this defect was specifically investigated for its stability upon prolonged electron-beam irradiation (200 kV). After 2 min its shape changed significantly (Figure 3 d). Sample beam interactions are not unusual in TEM, however the rearrangement of the crystal in the bombarded area is the signature of local energy differences in the samples. No "healing" of the defect could be observed.

Figure 3 e) and f) show visual differences of a structural defect depending on the TEM focus. While the
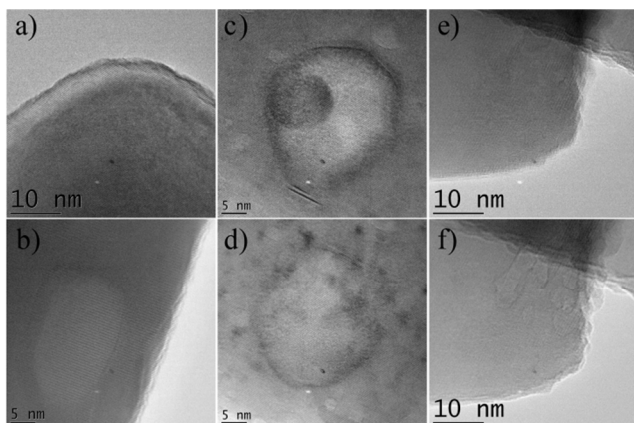
Figure 3. Detail TEM images of ZnO NRs. a) Tip of an as-grown ZnO NR. b) Detail of a structural defect of an annealed sample. c) Detail of a structural defect at the beginning of prolonged electron beam radiation (200 kV). d) The same detail as in c) but after 2 min of radiation. e) Tip of an annealed nanorod when in focus. f) The same detail as in e) but slightly out of focus, resolving structural defects.

investigated rod-tip was in focus in Figure 3 e) the image in Figure 3 f) shows the same detail slightly out of focus. In the focused image the structural defect is almost not visible. However, when slightly out of focus defects can be clearly observed. This is an important finding since it provides evidence that the defects are indeed locally determined and that one defect does not propagate throughout the entire rod.

Additional PL analysis, on samples annealed at 450 °C, was carried out in order to further investigate the nature of the A-line as well as the orange emission in the samples. Firstly, it is noted that during temperature dependent PL measurements the peak centre of the A-line shifted to lower energies with increasing temperature (red-shift, see Figure S6).The energy shift (in the range between 11.5 K and 120 K) is ca. 12.6 meV compared to 17.7 meV and 21.3 meV for the D_oX and FX_A transitions, respectively. If the A-line emission observed here was caused due to a free-to-bound (FB) transition – as suggested by various authors[56, 58, 60-63] – the slope of the peak position-shift as a function of temperature should be similar to the FX_A transition (after thermally correcting the A-line peak values).[56] However, for the samples examined in this study, the slope after the correction is still different (Figure S6 and related comments). In turn this may be taken as a first indication that the A-line transition in these samples is of a different nature.

From the temperature-variable PL measurements an activation energy E_A of 7.9 meV was estimated, which could be attributed to the dominant orange emission in the DLD range. However, compared to the NBE peaks this emission centre (ca. 1.9 eV) shows a blue-shift with increasing temperature (Figure S7). Interestingly a significant shift is only visible for temperatures > 100 K. If a shallow donor is assumed to be involved in the transition
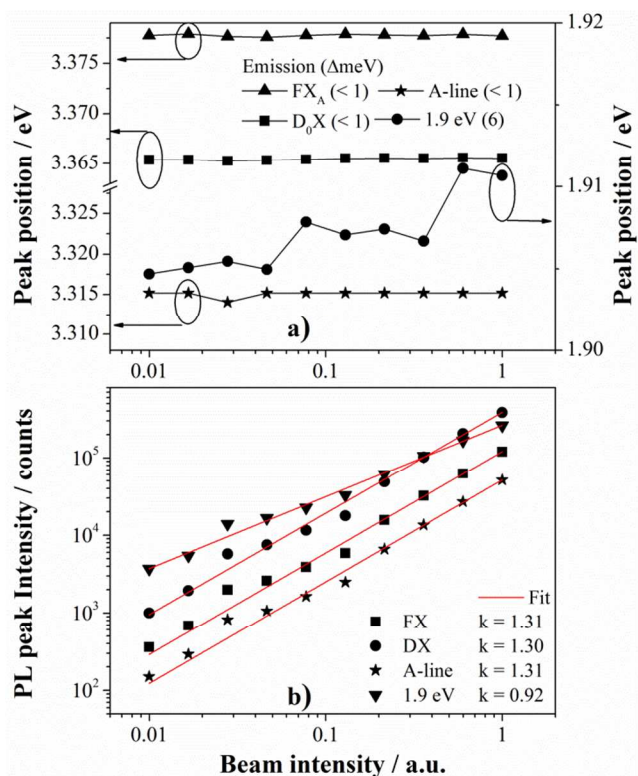

Figure 4. Peak position (a)) and peak intensity (b)) vs. laser-beam intensity for the NBE emissions and the orange emission (centered at 1.9 eV) recorded from LT-PL measurements at 11.5 K. The lines in a) are used as guidelines for the eyes.

it might be reasonable to expect thermalized electrons in the conduction band from these states at a specific temperature. As the recombination would then happen from the conduction band minimum (CBM) a blue-shift of the emission would occur, which could be partly compensated by the thermal shrinking of the bandgap.[57, 63] It is thus possible that the orange emission is dominated by the recombination between discrete defect states at lower temperatures but resembles a transition of an electron from the CBM into deep defect state with increasing temperature.

Secondly, PL measurements with varying laser intensity were recorded and the peak position of the PL emission (Figure 4 a)) and intensity (Figure 4 b)) were examined as a function of the beam intensity. In regards to the A-line emission of the NBE it was found that the peak position does not change significantly with varying beam intensity. In fact it can be seen that the change (< 1 meV) is similar to the FX_A and D_oX transitions. On the other hand a blue-shift of the peak position (6 meV) with increasing beam intensity has been observed for the defect-centre at 1.9 eV.

Similarly the peak intensity can be investigated in relation to the intensity of the laser beam. Since the beam intensity was only varied by two orders of magnitude, the power dependence of the luminescence can be described as $I \propto L^k$ (where I is the PL intensity, L the beam intensity

8

and k a coefficient) and can thus be computed as $I = aL^k$.[64, 65] Where a is a further coefficient. Free- and bound-excitonic transitions exhibit a coefficient k > 1. On the other hand, free-to-bound (FB) and donor-acceptor (DA) recombination processes progress with k < 1.[64, 65] The coefficient k has been determined to be 1.31, 1.30, 1.31, and 0.92 for the FX_A, D_oX, A-line and 1.9 eV transition, respectively.

The absence of a peak shift and an intensity change with k > 1 for the A-line emission as a function of the beam intensity rules out the possibility of a FB or DA transition as possible origin. Furthermore the intensity change is strikingly similar to the excitonic transitions (FX_A and D_oX). Since the appearance of the A-line emission and the structural defects are coincidental, it is thus postulated that the A-line emission in this study is related to the structural defects (bound-exciton at structural defects). That structural defects may be involved in this emission has been also proposed by others.[55, 58, 66] However, the temperature and beam intensity dependent PL results in this study are more in favor of a bound-excitonic nature, similar to the finding of Kurbanov et al. which found speck-like defects upon annealing of ZnO nanocrystals.[55]

Following the explanations above it also becomes obvious that the 1.9 eV defect emission must be of different origin – either of DA or FB nature. The observed blue-shift with increasing beam intensity may be taken as a fingerprint of a DA transition at low temperature. Since more donor-acceptor pairs are photo-excited the distance between the defects decreases, which in turn leads to a blue-shift with increasing beam intensity.[57, 67]

Finally, the evidence presented here further supports the hypothesis that the orange emission of these samples may originate from the kinetic formation of the V_O-Zn_i defect complex.[26, 49, 68] Theoretical calculations of the defect-complex have shown that the formation via a kick-out process leads to the shift of the Zn_i closer to/into the CBM while the V_O shifts closer to the valence band.[69, 70] Together with the evidence from the temperature-dependent PL measurements it is postulated that at low temperatures photo-luminescent transitions between these discrete defect states also contribute to the recorded signal. At room-temperature the recombination process is believed to happen mainly from the conduction band to the V_O state. Future research regarding the orange-luminescent defect centre is nevertheless needed. In particular electron paramagnetic resonance (EPR) measurements could prove highly valuable for the examination of the recombination mechanism but also for the evaluation of the photo-catalytic reactions and the involvement of intermediates.[71]

Based on the knowledge gained regarding the nature of the orange emission and the structural defects an assessment of the photo-catalytic properties of the defect-rich NR arrays cross-annealed in oxygen was carried out. The
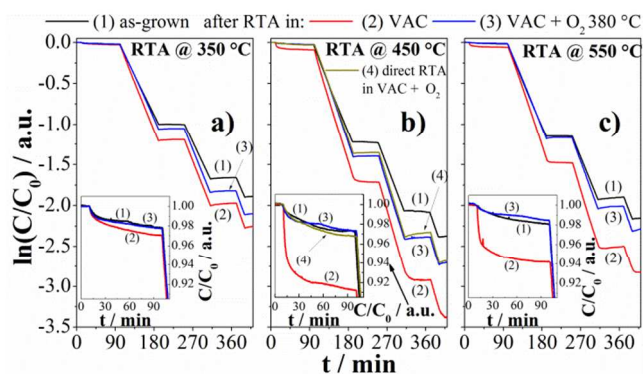

Figure 5. a)-c) dark dye-adsorption and photo-catalytic dye-degradation curves in methylene blue (MB) for samples before and after RTA in vacuum (VAC) at different temperatures + after cross-annealing in O_2 at 380 °C. Illumination intensity: 1 mW/cm². The insets magnify the change of MB concentration in the dark. b) also includes a sample which was only measured after receiving both RTA in VAC 450 °C + O_2 at 380 °C (trace (4)). Only samples measured after RTA in VAC 450 °C and 550 °C show strong dye adsorption.
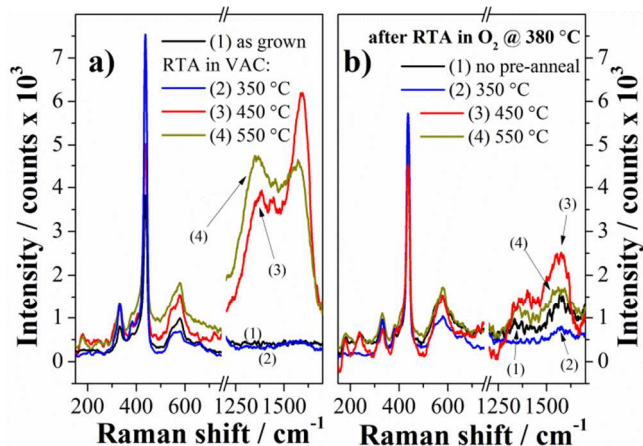

Figure 6. Raman spectra of samples annealed in vacuum at different temperatures before (a)) and after (b)) cross-annealing in O_2 at 380 °C. After cross-annealing in O_2 at 380 °C the intensity of carbon related modes (e.g. graphitic shell) decreases dramatically.

dye-degradation spectra together with the Raman spectra of the samples before and after annealing in oxygen are shown in Figure 5 and Figure 6, respectively. Investigating the behavior of the samples in the dark first, no strong dark dye-adsorption could be observed for the sample annealed at 350 °C (Figure 5 a)). However, strong dye-adsorption in the dark was again present for the strong orange emitting sample (450 °C in Figure 5 b), also compare to Figure 1d)) but was also seen for the sample annealed in vacuum at 550 °C (Figure 5 c)).

Interestingly cross-annealing in oxygen destroys the strong dark dye-adsorption for these samples. The same holds true for a sample that had been not tested for its photo-catalytic performance prior to RTA in vacuum at 450 °C + O_2 at 380 °C (trace (4) in Figure 5 b)).

9

To evaluate these effects, annealed samples were measured for their Raman responses after each RTA step. As can be seen from Figure 6 a), only annealing conditions that lead to strong dark dye-adsorption (450 °C and 550 °C) also result in the appearance of intense carbon-related modes in the Raman. However, these modes are dramatically decreased upon the cross-annealing step in O_2 at 380 °C (Figure 6 b)).

As elucidated in the first part of the paper, the carbon-related modes cannot be attributed to any of the observed PL emissions (including the observed structural defects). More so these features are found to be annealing atmosphere and temperature dependent. Thus it is postulated that annealing in vacuum at elevated temperatures (> 400 °C) leads to diffusion of carbon from the bulk of the rods towards the surface, forming a graphitic structure (e.g. overlayer/shell). An additional RTA step in O_2 then results in "burning off" of these structures. In turn it becomes clear that the strong dark dye-adsorption of MB is directly correlated to the graphitic structure which must exhibit a negative charge.

Importantly a charged surface could lead to a better degradation of pollutants due to an increased attraction of same towards the nanorod-surface. Hence, when evaluating the influence of a particular deep-level defect on the photo-catalytic performance one has to pay extra attention to a possible interplay and synergy between the defect and possible surface effects. When both contribute to the photo-catalytic performance a direct correlation to the effect of the deep-level defect may not be established. In the present study this problem has been tackled by cross-annealing the samples in oxygen. Furthermore it is noteworthy that the dye adsorption effect is diminished after several subsequent measurements.

Regarding the photo-catalytic dye-degradation all samples show an improvement (i.e. increased degradation rate) after the respective RTA in vacuum ((2) traces in Figure 5). However, it should be noticed that that sample annealed at 450 °C (strong orange emission) shows a larger improvement compared to samples annealed at 350 °C or 550 °C.

As mentioned above, it may be possible that an interplay between the strong dye-adsorption and the orange-luminescent defects leads to the enhanced degradation characteristics. An indication for this may be seen in the reduction of the degradation rate upon cross-annealing in oxygen. Based on the performance after cross-annealing, the apparent quantum efficiency (number of degraded dye molecules/number of incident photons) was estimated to be ca. 36.7 % (first light-on stage). Although the degradation rate decreases after cross annealing, the orange luminescent sample still shows an overall improvement of the photo-catalytic performance when compared to the as-grown measurement – a behaviour which was also observed when MO was used as a dye (see Figure S8). This is not as clearly seen for the samples which were sub-

ject to RTA in vacuum at 350 °C or 550 °C prior to the cross-annealing step. In addition to the removal of carbon the cross-annealing in oxygen could therefore also play a crucial role in terms of the defect chemistry. It is reasonable to expect a certain filling of oxygen vacancies upon this treatment (see also decreased DLD emission at ca. 2.5 eV after cross-annealing in oxygen for the sample subjected to RTA in vacuum at 550 °C - Figure 2 d)), which in turn could lead to a reduced dye-degradation since oxygen vacancies have been reported to aid same.[23, 47] However, under the assumption that higher temperatures during the RTA in vacuum lead to a higher number of oxygen vacancies it can be expected that the orange-luminescent defects (V_O-Zn_i defect-complex) are indeed a major contributor to the enhanced photo-catalytic performance for the sample annealed in vacuum at 450 °C. These results are in line with previous experimental evidences that suggest that the orange-luminescent defect centres act as slow electron traps which prolong the hole lifetime and therefore increase the possibility to run photo-chemical reactions.

Conclusions

A simple, low-temperature solution-based growth method was used to grow intentionally defect-rich ZnO NR arrays. While keeping variables such as growth conditions/technique and morphology unchanged a careful analysis of the material properties and resulting photo-catalytic performance of rapid thermally annealed ZnO nanorod-arrays was carried out. The presence of various defects could be confirmed with structural defects, strong orange emission and a graphitic structure (e.g shell) dominating the material properties. Inherent to all annealed samples (T_{RTA} 350 °C – 550 °C) is the appearance of structural defects, which were attributed to the PL emission at ca. 3.31 eV. No direct influence on the photo-catalytic performance could be established for these defects. Rapid thermal annealing at 450 °C in vacuum gave rise to strong orange defect emission. Building on an earlier study, further evidence has been provided that the orange emission in the samples is caused by the V_O-Zn_i defect-complex. Interestingly, these samples showed strong dye-adsorption and an improvement of the photo-catalytic dye-degradation. The experimental studies suggest that a graphitic structure (e.g. shell) is responsible for the dark adsorption. In turn this may enforce the dye-degradation by orange-luminescent samples due to the attraction of MB towards the sample surface as a result of the graphitic structure.

Finally some more general conclusions regarding the assessment of photo-catalytic properties of defect-rich materials can be drawn from the specific findings of this study. Firstly, a comparison between different morphologies and/or growth methods is troublesome unless the defect chemistry is similar. Secondly, the significance of other possible contributions (e.g. surface-functionality and polarity, nature of the dye, other defects) needs to be

10

1
2
3
4
5
6
7
8
9
10
11
12
13
14
15
16
17
18
19
20
21
22
23
24
25
26
27
28
29
30
31
32
33
34
35
36
37
38
39
40
41
42
43
44
45
46
47
48
49
50
51
52
53
54
55
56
57
58
59
60

evaluated prior to assessing the influence of a specific defect. Whenever possible, appropriate post-deposition treatments (e.g. cross-annealing, plasma- and surface treatment) should be used to help minimize these contributions. Finally, an interplay of intrinsic defects – which can mask the real contribution of a specific defect –must be expected when various defect centres are present in the material.

AUTHOR INFORMATION

Corresponding Author

* Corresponding author: jan.kegel@tyndall.ie

Author Contributions

J.K. designed the experiments in correspondence with M.E.P. J.K. conducted the experiments with the help of V.Z.Z (LT-PL) and M.S. (TEM). J.K. wrote the manuscript. The manuscript was finalized through contributions of all authors.

SUPPORTING INFORMATION

Dye-degradation rates for samples presented in Figure 1 and Figure 5; Absorbance spectra of MB, MO and a representative ZnO NR array; Materials characterization of as-grown samples; Example of a fitted low-temperature PL spectrum; XPS spectrum of a ZnO NR array annealed in vacuum at 450 °C; High-resolution XRD patterns, SEM images and room-temperature PL spectra of a sample subjected to low-temperature long-term annealing and RTA in forming gas; Temperature-dependent PL measurements and Arrhenius fit; Integrated PL intensity and PL peak position of the orange emission (1.9 eV) as a function of the inverse temperature; MO degradation curve and rate determination for a sample annealed in VAC at 450 °C and VAC at 450 C + O_2 at 380 °C.

References

1.   Chang, C. M.; Hon, M. H.; Leu, I. C., Preparation of ZnO nanorod arrays with tailored defect-related characterisitcs and their effect on the ethanol gas sensing performance. *Sensors and Actuators B: Chemical* **2010,** 151, (1), 15-20.
2.   Zhang, Y.; Ram, M. K.; Stefanakos, E. K.; Goswami, D. Y., Synthesis, Characterization, and Applications of ZnO Nanowires. *Journal of Nanomaterials* **2012,** 2012, 1-22.

3.   Echresh, A.; Chey, C. O.; Shoushtari, M. Z.; Nur, O.; Willander, M., Tuning the emission of ZnO nanorods based light emitting diodes using Ag doping. *Journal of Applied Physics* **2014,** 116, (19), No. 193104.
4.   Lee, S. W.; Cho, H. D.; Panin, G.; Won Kang, T., Vertical ZnO nanorod/Si contact light-emitting diode. *Applied Physics Letters* **2011,** 98, (9), No. 093110.
5.   Hwang, S.-H.; Chung, T.-H.; Lee, B.-T., Study on the interfacial layer in ZnO/GaN heterostructure light-emitting diode. *Materials Science and Engineering: B* **2009,** 157, (1-3), 32-35.
6.   Könenkamp, R.; Word, R. C.; Godinez, M., Ultraviolet Electroluminescence from ZnO/Polymer Heterojunction Light-Emitting Diodes. *Nano Letters* **2005,** 5, (10), 2005-2008.
7.   Garcia-Alonso, D.; Smit, S.; Bordihn, S.; Kessels, W. M. M., Silicon passivation and tunneling contact formation by atomic layer deposited Al2O3/ZnO stacks. *Semiconductor Science and Technology* **2013,** 28, (8), No. 082002.
8.   Smit, S.; Garcia-Alonso, D.; Bordihn, S.; Hanssen, M. S.; Kessels, W. M. M., Metal-oxide-based hole-selective tunneling contacts for crystalline silicon solar cells. *Solar Energy Materials and Solar Cells* **2014,** 120, 376-382.
9.   Xu, S.; Wang, Z. L., One-dimensional ZnO nanostructures: Solution growth and functional properties. *Nano Research* **2011,** 4, (11), 1013-1098.
10.   Liu, F.; Guo, M. Y.; Leung, Y. H.; Djurišić, A. B.; Ng, A. M. C.; Chan, W. K., Effect of starting properties and annealing on photocatalytic activity of ZnO nanoparticles. *Applied Surface Science* **2013,** 283, 914-923.
11.   Liu, F.; Leung, Y. H.; Djurišić, A. B.; Ng, A. M. C.; Chan, W. K., Native Defects in ZnO: Effect on Dye Adsorption and Photocatalytic Degradation. *The Journal of Physical Chemistry C* **2013,** 117, (23), 12218-12228.
12.   Liu, M.; Nam, C.-Y.; Black, C. T.; Kamcev, J.; Zhang, L., Enhancing Water Splitting Activity and Chemical Stability of Zinc Oxide Nanowire Photoanodes with Ultrathin Titania Shells. *The Journal of Physical Chemistry C* **2013,** 117, (26), 13396-13402.
13.   Ranjith, K. S.; Pandian, R.; McGlynn, E.; Rajendra Kumar, R. T., Alignment, Morphology and Defect Control of Vertically Aligned ZnO Nanorod Array: Competition between "Surfactant" and "Stabilizer" Roles of the Amine Species and Its Photocatalytic Properties. *Crystal Growth & Design* **2014,** 14, (6), 2873-2879.
14.   Kayaci, F.; Vempati, S.; Donmez, I.; Biyikli, N.; Uyar, T., Role of zinc interstitials and oxygen vacancies of ZnO in photocatalysis: a bottom-up approach to control defect density. *Nanoscale* **2014,** 6, (17), 10224-10234.
15.   Cai, L.; Ren, F.; Wang, M.; Cai, G.; Chen, Y.; Liu, Y.; Shen, S.; Guo, L., V ions implanted ZnO nanorod arrays for photoelectrochemical water splitting under visible light. *International Journal of Hydrogen Energy* **2015,** 40, (3), 1394-1401.
16.   Janotti, A.; Van de Walle, C. G., Fundamentals of zinc oxide as a semiconductor. *Reports on Progress in Physics* **2009,** 72, (12), No. 126501.
17.   Djurišić, A. B.; Ng, A. M. C.; Chen, X. Y., ZnO nanostructures for optoelectronics: Material properties and device applications. *Progress in Quantum Electronics* **2010,** 34, (4), 191-259.
18.   Papari, G. P.; Silvestri, B.; Vitiello, G.; De Stefano, L.; Rea, I.; Luciani, G.; Aronne, A.; Andreone, A., Morphological, Structural, and Charge Transfer Properties of F-Doped ZnO: A Spectroscopic Investigation. *The Journal of Physical Chemistry C* **2017,** 121, (29), 16012-16020.

11

19.   Al-Sabahi, J.; Bora, T.; Al-Abri, M.; Dutta, J., Controlled Defects of Zinc Oxide Nanorods for Efficient Visible Light Photocatalytic Degradation of Phenol. *Materials* **2016,** 9, (4), 238-247.

20.   Wang, J.; Wang, Z.; Huang, B.; Ma, Y.; Liu, Y.; Qin, X.; Zhang, X.; Dai, Y., Oxygen vacancy induced band-gap narrowing and enhanced visible light photocatalytic activity of ZnO. *ACS Appl Mater Interfaces* **2012,** 4, (8), 4024-4030.

21.   Kumar, S. G.; Rao, K. S. R. K., Zinc oxide based photocatalysis: tailoring surface-bulk structure and related interfacial charge carrier dynamics for better environmental applications. *RSC Adv.* **2015,** 5, (5), 3306-3351.

22.   Zhang, X.; Qin, J.; Xue, Y.; Yu, P.; Zhang, B.; Wang, L.; Liu, R., Effect of aspect ratio and surface defects on the photocatalytic activity of ZnO nanorods. *Sci Rep* **2014,** 4, No. 4596.

23.   Wang, J.; Liu, P.; Fu, X.; Li, Z.; Han, W.; Wang, X., Relationship between Oxygen Defects and the Photocatalytic Property of ZnO Nanocrystals in Nafion Membranes. *Langmuir* **2009,** 25, (2), 1218-1223.

24.   Warule, S. S.; Chaudhari, N. S.; Kale, B. B.; More, M. A., Novel sonochemical assisted hydrothermal approach towards the controllable synthesis of ZnO nanorods, nanocups and nanoneedles and their photocatalytic study. *CrystEngComm* **2009,** 11, (12), 2776-2783.

25.   Baruah, S.; Sinha, S. S.; Ghosh, B.; Pal, S. K.; Raychaudhuri, A. K.; Dutta, J., Photoreactivity of ZnO nanoparticles in visible light: Effect of surface states on electron transfer reaction. *Journal of Applied Physics* **2009,** 105, (7), No. 074308.

26.   Kegel, J.; Laffir, F.; Povey, I. M.; Pemble, M. E., Defect-promoted photo-electrochemical performance enhancement of orange-luminescent ZnO nanorod-arrays. *Phys Chem Chem Phys* **2017,** 19, (19), 12255--12268.

27.   Mills, A.; O'Rourke, C., Adsorption and Destruction of Methylene Blue by Semiconductor Photocatalysis. *Green* **2011,** 1, (1), 105-113.

28.   Yan, X.; Ohno, T.; Nishijima, K.; Abe, R.; Ohtani, B., Is methylene blue an appropriate substrate for a photocatalytic activity test? A study with visible-light responsive titania. *Chemical Physics Letters* **2006,** 429, (4-6), 606-610.

29.   Bae, S.; Kim, S.; Lee, S.; Choi, W., Dye decolorization test for the activity assessment of visible light photocatalysts: Realities and limitations. *Catalysis Today* **2014,** 224, 21-28.

30.   Chen, T.; Zheng, Y.; Lin, J. M.; Chen, G., Study on the photocatalytic degradation of methyl orange in water using Ag/ZnO as catalyst by liquid chromatography electrospray ionization ion-trap mass spectrometry. *J Am Soc Mass Spectrom* **2008,** 19, (7), 997-1003.

31.   Guo, M. Y.; Ng, A. M. C.; Liu, F.; Djurišić, A. B.; Chan, W. K.; Su, H.; Wong, K. S., Effect of Native Defects on Photocatalytic Properties of ZnO. *The Journal of Physical Chemistry C* **2011,** 115, (22), 11095-11101.

32.   Kaur, J.; Bansal, S.; Singhal, S., Photocatalytic degradation of methyl orange using ZnO nanopowders synthesized via thermal decomposition of oxalate precursor method. *Physica B: Condensed Matter* **2013,** 416, 33-38.

33.   Wang, Y.; Shi, R.; Lin, J.; Zhu, Y., Enhancement of photocurrent and photocatalytic activity of ZnO hybridized with graphite-like C3N4. *Energy & Environmental Science* **2011,** 4, (8), 2922–2929.

34.   Mills, A.; Wang, J., Photobleaching of methylene blue sensitised by TiO2: an ambiguous system? *Journal of Photochemistry and Photobiology A: Chemistry* **1999,** 127, (1–3), 123-134.

35.   Imran, M.; Yousaf, A. B.; Zhou, X.; Liang, K.; Jiang, Y. F.; Xu, A. W., Oxygen-Deficient TiO2-x/Methylene Blue Colloids: Highly Efficient Photoreversible Intelligent Ink. *Langmuir* **2016,** 32, (35), 8980-8987.

36.   Ranjith, K. S.; Rajendra Kumar, R. T., Regeneration of an efficient, solar active hierarchical ZnO flower photocatalyst for repeatable usage: controlled desorption of poisoned species from active catalytic sites. *RSC Advances* **2017,** 7, (9), 4983-4992.

37.   Baruah, S.; Dutta, J., Hydrothermal growth of ZnO nanostructures. *Science and Technology of Advanced Materials* **2009,** 10, (1), No. 013001.

38.   Kuriakose, S.; Satpati, B.; Mohapatra, S., Enhanced photocatalytic activity of Co doped ZnO nanodisks and nanorods prepared by a facile wet chemical method. *Phys Chem Chem Phys* **2014,** 16, (25), 12741-12749.

39.   Mishra, D. K.; Mohapatra, J.; Sharma, M. K.; Chattarjee, R.; Singh, S. K.; Varma, S.; Behera, S. N.; Nayak, S. K.; Entel, P., Carbon doped ZnO: Synthesis, characterization and interpretation. *Journal of Magnetism and Magnetic Materials* **2013,** 329, 146-152.

40.   Vernardou, D.; Kenanakis, G.; Couris, S.; Manikas, A. C.; Voyiatzis, G. A.; Pemble, M. E.; Koudoumas, E.; Katsarakis, N., The effect of growth time on the morphology of ZnO structures deposited on Si (100) by the aqueous chemical growth technique. *Journal of Crystal Growth* **2007,** 308, (1), 105-109.

41.   Windisch, C. F.; Exarhos, G. J.; Yao, C.; Wang, L.-Q., Raman study of the influence of hydrogen on defects in ZnO. *Journal of Applied Physics* **2007,** 101, (12), No. 123711.

42.   He, X.; Yang, H.; Chen, Z.; Liao, S. S. Y., Effect of Co-doping content on hydrothermal derived ZnO array films. *Physica B: Condensed Matter* **2012,** 407, (15), 2895-2899.

43.   Tu, N.; Nguyen, K. T.; Trung, D. Q.; Tuan, N. T.; Do, V. N.; Huy, P. T., Effects of carbon on optical properties of ZnO powder. *Journal of Luminescence* **2016,** 174, 6-10.

44.   Liu, X.; Du, H.; Sun, X. W.; Liu, B.; Zhao, D.; Sun, H., Visible-light photoresponse in a hollow microtube–nanowire structure made of carbon-doped ZnO. *CrystEngComm* **2012,** 14, (8), 2886–2890.

45.   Khanderi, J.; Hoffmann, R. C.; Gurlo, A.; Schneider, J. J., Synthesis and sensoric response of ZnO decorated carbon nanotubes. *Journal of Materials Chemistry* **2009,** 19, (28), 5039–5046.

46.   Katumba, G.; Mwakikunga, B. W.; Mothibinyane, T. R., FTIR and Raman Spectroscopy of Carbon Nanoparticles in SiO2, ZnO and NiO Matrices. *Nanoscale Research Letters* **2008,** 3, (11), 421-426.

47.   Kayaci, F.; Vempati, S.; Ozgit-Akgun, C.; Biyikli, N.; Uyar, T., Enhanced photocatalytic activity of homoassembled ZnO nanostructures on electrospun polymeric nanofibers: A combination of atomic layer deposition and hydrothermal growth. *Applied Catalysis B: Environmental* **2014,** 156-157, 173-183.

48.   Xie, R.; Sekiguchi, T.; Ishigaki, T.; Ohashi, N.; Li, D.; Yang, D.; Liu, B.; Bando, Y., Enhancement and patterning of ultraviolet emission in ZnO with an electron beam. *Applied Physics Letters* **2006,** 88, (13), No. 134103.

49.   Djurišić, A. B.; Leung, Y. H.; Tam, K. H.; Hsu, Y. F.; Ding, L.; Ge, W. K.; Zhong, Y. C.; Wong, K. S.; Chan, W. K.; Tam, H. L.; Cheah, K. W.; Kwok, W. M.; Phillips, D. L., Defect emissions in ZnO nanostructures. *Nanotechnology* **2007,** 18, (9), No. 095702.

12

50. Sekiguchi, T.; Ohashi, N.; Terada, Y., Effect of Hydrogenation on ZnO Luminescence. *Japanese Journal of Applied Physics* **1997,** 36, (3A), L289-L291.

51. Ohashi, N.; Ishigaki, T.; Okada, N.; Sekiguchi, T.; Sakaguchi, I.; Haneda, H., Effect of hydrogen doping on ultraviolet emission spectra of various types of ZnO. *Applied Physics Letters* **2002,** 80, (16), 2869-2871.

52. Bora, T.; Sathe, P.; Laxman, K.; Dobretsov, S.; Dutta, J., Defect engineered visible light active ZnO nanorods for photocatalytic treatment of water. *Catalysis Today* **2017,** 284, 11-18.

53. Teke, A.; Özgür, Ü.; Doğan, S.; Gu, X.; Morkoç, H.; Nemeth, B.; Nause, J.; Everitt, H. O., Excitonic fine structure and recombination dynamics in single-crystalline ZnO. *Physical Review B* **2004,** 70, (19), No. 195207.

54. Meyer, B. K.; Alves, H.; Hofmann, D. M.; Kriegseis, W.; Forster, D.; Bertram, F.; Christen, J.; Hoffmann, A.; Straßburg, M.; Dworzak, M.; Haboeck, U.; Rodina, A. V., Bound exciton and donor–acceptor pair recombinations in ZnO. *physica status solidi (b)* **2004,** 241, (2), 231-260.

55. Kurbanov, S. S.; Panin, G. N.; Kang, T. W., Spatially resolved investigations of the emission around 3.31 eV (A-line) from ZnO nanocrystals. *Applied Physics Letters* **2009,** 95, (21), No. 211902.

56. Liu, K. W.; Chen, R.; Xing, G. Z.; Wu, T.; Sun, H. D., Photoluminescence characteristics of high quality ZnO nanowires and its enhancement by polymer covering. *Applied Physics Letters* **2010,** 96, (2), No. 023111.

57. Yang, Z.; Liu, J. L., Donor-acceptor-pair photoluminescence in Ga-doped ZnO thin films grown by plasma-assisted molecular beam epitaxy. *Journal of Vacuum Science & Technology B, Nanotechnology and Microelectronics: Materials, Processing, Measurement, and Phenomena* **2010,** 28, (3), C3D6-C3D9.

58. Schirra, M.; Schneider, R.; Reiser, A.; Prinz, G. M.; Feneberg, M.; Biskupek, J.; Kaiser, U.; Krill, C. E.; Thonke, K.; Sauer, R., Stacking fault related3.31–eVluminescence at130–meVacceptors in zinc oxide. *Physical Review B* **2008,** 77, (12), No. 125215.

59. Wagner, M. R.; Zimmer, P.; Hoffmann, A.; Thomsen, C., Resonant Raman scattering at exciton intermediate states in ZnO. *physica status solidi (RRL) – Rapid Research Letters* **2007,** 1, (5), 169-171.

60. Zhang, B. P.; Binh, N. T.; Segawa, Y.; Wakatsuki, K.; Usami, N., Optical properties of ZnO rods formed by metalorganic chemical vapor deposition. *Applied Physics Letters* **2003,** 83, (8), 1635-1637.

61. Zhao, Q. X.; Willander, M.; Morjan, R. E.; Hu, Q. H.; Campbell, E. E. B., Optical recombination of ZnO nanowires grown on sapphire and Si substrates. *Applied Physics Letters* **2003,** 83, (1), 165-167.

62. Wang, Q.; Yan, Y.; Zeng, Y.; Lu, Y.; Chen, L.; Jiang, Y., Free-Standing Undoped ZnO Microtubes with Rich and Stable Shallow Acceptors. *Sci Rep* **2016,** 6, No. 27341.

63. He, H.; Yang, Q.; Liu, C.; Sun, L.; Ye, Z., Size-Dependent Surface Effects on the Photoluminescence in ZnO Nanorods. *The Journal of Physical Chemistry C* **2011,** 115, (1), 58-64.

64. Schmidt, T.; Lischka, K.; Zulehner, W., Excitation-power dependence of the near-band-edge photoluminescence of semiconductors. *Physical Review B* **1992,** 45, (16), 8989-8994.

65. Gadallah, A.-S.; El-Nahass, M. M., Structural, Optical Constants and Photoluminescence of ZnO Thin Films Grown by Sol-Gel Spin Coating. *Advances in Condensed Matter Physics* **2013,** 2013, 1-11.

66. Morrison, J. L.; Huso, J.; Hoeck, H.; Casey, E.; Mitchell, J.; Bergman, L.; Norton, M. G., Optical properties of ZnO and MgZnO nanocrystals below and at the phase separation range. *Journal of Applied Physics* **2008,** 104, (12), No. 123519.

67. Tamura, K.; Makino, T.; Tsukazaki, A.; Sumiya, M.; Fuke, S.; Furumochi, T.; Lippmaa, M.; Chia, C. H.; Segawa, Y.; Koinuma, H.; Kawasaki, M., Donor–acceptor pair luminescence in nitrogen-doped ZnO films grown on lattice-matched ScAlMgO4 (0001) substrates. *Solid State Communications* **2003,** 127, (4), 265-269.

68. Tam, K. H.; Cheung, C. K.; Leung, Y. H.; Djurišić, A. B.; Ling, C. C.; Beling, C. D.; Fung, S.; Kwok, W. M.; Chan, W. K.; Phillips, D. L.; Ding, L.; Ge, W. K., Defects in ZnO Nanorods Prepared by a Hydrothermal Method. *The Journal of Physical Chemistry B* **2006,** 110, (42), 20865-20871.

69. Kim, D.-H.; Lee, G.-W.; Kim, Y.-C., Interaction of zinc interstitial with oxygen vacancy in zinc oxide: An origin of n-type doping. *Solid State Communications* **2012,** 152, (18), 1711-1714.

70. Kim, Y.-S.; Park, C. H., Rich Variety of Defects in ZnO via an Attractive Interaction between O Vacancies and Zn Interstitials: Origin ofn-Type Doping. *Physical Review Letters* **2009,** 102, (8), No. 086403.

71. Vitiello, G.; Pezzella, A.; Calcagno, V.; Silvestri, B.; Raiola, L.; D'Errico, G.; Costantini, A.; Branda, F.; Luciani, G., 5,6-Dihydroxyindole-2-carboxylic Acid–TiO2 Charge Transfer Complexes in the Radical Polymerization of Melanogenic Precursor(s). *The Journal of Physical Chemistry C* **2016,** 120, (11), 6262-6268.
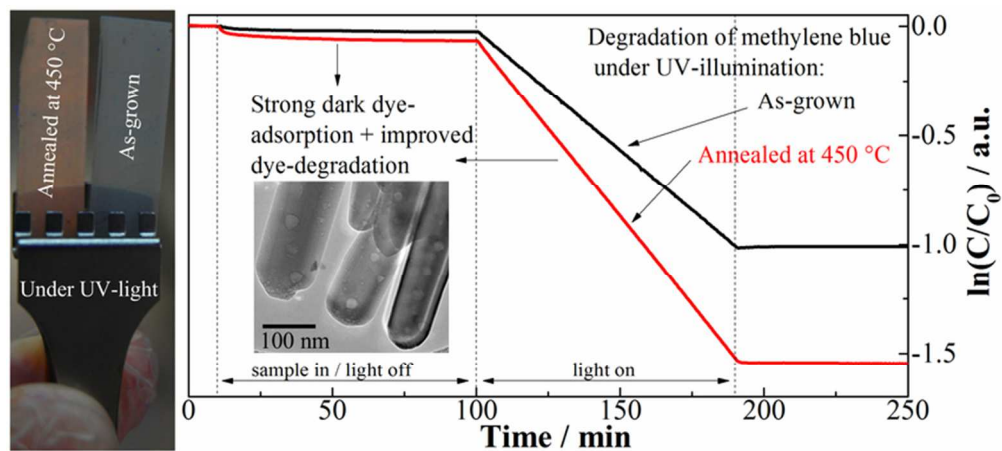
13

Table of contents graphic

35x16mm (600 x 600 DPI)